J. Fluid Mech. (2008), *vol.* 610, *pp.* 261–284.
doi:10.1017/S0022112008002760 Printed in the United Kingdom

On the Lamb vector divergence in Navier–Stokes flows

CURTIS W. HAMMAN[1]†, JOSEPH C. KLEWICKI[2] AND ROBERT M. KIRBY[1,3]

[1]Scientific Computing and Imaging Institute, University of Utah, Salt Lake City, UT 84112, USA
[2]Department of Mechanical Engineering, University of New Hampshire, Durham, NH 03824, USA
[3]School of Computing, University of Utah, Salt Lake City, UT 84112, USA

(Received 10 May 2007 and in revised form 27 May 2008)

The mathematical and physical properties of the Lamb vector divergence are explored. Toward this aim, the instantaneous and mean dynamics of the Lamb vector divergence are examined in several analytic and turbulent flow examples relative to its capacity to identify and characterize spatially localized motions having a distinct capacity to effect a time rate of change of momentum. In this context, the transport equation for the Lamb vector divergence is developed and shown to accurately describe the dynamical mechanisms by which adjacent high- and low-momentum fluid parcels interact to effect a time rate of change of momentum and generate forces such as drag. From this, a transport-equation-based framework is developed that captures the self-sustaining spatiotemporal interactions between coherent motions, e.g. ejections and sweeps in turbulent wall flows, as predicted by the binary source–sink distribution of the Lamb vector divergence. New insight into coherent motion development and evolution is found through the analysis of the Lamb vector divergence.

1. Introduction

The objective of the present paper is to explore the properties of the Lamb vector divergence and the transport equation for this variable. The motivation to do so stems from the close connection between the Lamb vector divergence and the motions in a flow, especially those instantaneous motions in turbulent flows, having a distinctively high capacity to effect a time rate of change of momentum. This specific attribute underlies the hypothesis that through the study of the Lamb vector, its divergence and transport, one may construct a rigorous (transport-equation-based) methodology for the study of what are generically referred to as coherent motions. To provide a context in this regard, the challenges associated with the various approaches to the turbulence problem and, in particular, coherent motion research are briefly reviewed.

Early approaches to the turbulence problem focused on the observation that the instantaneous time trace from a sensor placed in the flow (e.g. a hot-wire probe) appeared essentially random. From this perspective, the classical statistical theories of turbulence emerged, e.g. Taylor (1935), Batchelor (1953), Monin & Yaglom (1977). Of course, associated with this approach is the well-known closure problem for the Reynolds stress gradient term in the time-averaged momentum equation or the unclosed higher-order terms in Kármán–Howarth-type equations (Hinze 1975). Despite these challenges, a primary advantage of the statistical approach is its

† Present address: Center for Turbulence Research, Stanford University, Stanford, CA, USA.

relatively direct connections to the underlying equations of motion. On the other hand, a primary shortcoming is that by their very nature these approaches provide diminished insight into the underlying instantaneous dynamics. This shortcoming has a very practical ramification since, even though applications may only require a net time-averaged result or answer, in actual practice one must contend with the instantaneous flow field. Thus, an understanding of how the average flow field is established from the ensemble of the instantaneous flow field realizations is required.

Starting about fifty years ago, the purely stochastic perspective began to be modified through the recognition that within essentially all turbulent flows (and especially turbulent shear flows) there exist coherent motions† that, relative to the volume of flow they occupy and the duration over which they act, are responsible for disproportionate contributions to the overall momentum transport. Early coherent motion research was significantly aided by the development of flow visualization techniques that provided spatial information relating to instantaneous flow evolution. Of course, significant care must be taken when a visualization marker is used as a surrogate since, for example, the diffusion coefficients of commonly employed visualization markers tend to be significantly different from the fluid viscosity. Placing such challenges aside, the primary goal of coherent motion research continues to rest in the notion that within the totality of motions (governed by the Navier–Stokes equations) there exists a special subset of eddies that carry with them the bulk of the dynamics. Implicit to this approach is the subjectivity associated with the notion that the motions that look most 'organized' are the coherent motions. Of course, a disadvantage to coherent motion research is that the veracity of this assumption must be tested empirically to determine whether the motions identified are, in fact, especially dynamically significant. At the heart of this challenge resides the fact that, at present, there are no rigorously established equations that selectively describe the dynamics of coherent motions.

One methodology that seeks to address this challenge involves the construction of low-dimensional dynamical models. That is, consistent with the idea that the bulk of the dynamics resides with the coherent motions is the mathematical notion that within the phase space containing the trajectories of a high-dimensional system there may exist much lower-dimensional manifolds that capture most of the important dynamics. In this regard, proper orthogonal decomposition (Lumley 1967; Berkooz, Holmes & Lumley 1993) and stochastic estimation (Adrian & Moin 1988) methods are most often used to construct the energetically most significant eigenmodes for which dynamical evolution equations are subsequently developed (Aubry *et al.* 1988). This approach has been applied to a wide variety of flow fields (Bakewell & Lumley 1967; Chambers *et al.* 1988; Berkooz, Holmes & Lumley 1991), and in some cases with apparently considerable success. Persistent issues regarding this approach, however, relate to the criteria by which the full system is truncated to form the low-dimensional model. Namely, how should the modes be selected, and how many modes are enough? Particularly bothersome in this regard is that these criteria are almost exclusively based upon the fraction of the total energy contained in the projected modes. The relationship between the amount of energy realized via the low-dimensional model and that which is sufficient to capture the important dynamics is, however, an uncertain proposition since causality is embodied in the dynamics from which the energetics result.

† Note that in the present study the term 'coherent structure' will be avoided, since the word 'structure' carries with it the undue suggestion of a permanence of form.

A central and long-held concept of coherent motion research relates to the importance of vortices, e.g. Robinson (1991), Jeong & Hussain (1995), Chakraborty, Balachandar & Adrian (2005). Traditionally, the notion of a vortex focuses on a specific type of vorticity bearing motion that has nominally circular and closed streamlines when viewed in cross-section within an appropriately advecting reference frame. The special importance attributed to such motions is implicit to a very large volume of turbulence research – evoking the often cited anthropomorphic characterization that vortices are 'the sinews and muscles of turbulence' (Küchemann 1965). A universally accepted definition of a vortex, however, does not exist. Still, with the advent of full field information via direct numerical simulation (DNS) and particle image velocimetry (PIV), increasingly mathematically sophisticated methods for the identification and classification of vortices have been proposed and continue to be developed. There are, however, unanswered yet fundamental questions worth asking that relate to the efficacy of this course of investigation. For example, why should one focus on the characteristics of nominally closed streamlines in cross-section when there is little *a priori* dynamical justification for imposing such a constraint? Similarly, what (if any) reliable connection exists between the general concept of a vortex and the flow dynamics as, for example, reflected by or related to the equations of motion? Indeed, recent definitions (e.g. Chakraborty *et al.* 2005) as well as those given in virtually all previous studies attempting to define a vortex contain no (or very little) explicit requirement for a vortex to have any special dynamical significance. That being the case, it seems appropriate to question whether the elevated significance specifically attributed to vortices is entirely rational.

Though coherent motions are often discussed relative to embedded vortices, there are good reasons to believe that the notion is both unduly restrictive while simultaneously in need of extension. For example, the studies by Brasseur & Lin (2005) arrived at important conclusions relating to the detection and characterization of highly active regions of vorticity, strain rate and Reynolds stress. Relative to overall dynamical significance, they found that regions of high-intensity vorticity (for example) were not necessarily more important than adjacent lower-intensity regions; similar results were also found by Tsinober (1998). Rather, the overarching conclusion was that, owing to the complex interactions over a wide range of scales (especially in well-developed as opposed to post-transitional turbulent flows), a clear connection between the important dynamics and any particular class of motion is not at all apparent. In addition, they showed that tube-like concentrations of vorticity were not quantitatively any more significant than sheet-like concentrations. A clear result derived from their findings is that, while the instantaneous local flow domains that play a disproportionate role (relative to the volume they occupy) in local momentum transport often contain vortices, significant care should be taken in attributing vortices as the causal mechanism carrying the dynamics. In the end, searching out and tracking coherent vortices is likely to have only limited success relative to educing robust models of flow physics.

The present work asserts that there are advantages to directly connecting the attributes of coherent motions to field variables, and demanding that the particular variables chosen reflect a distinct capacity to effect a time rate of change of momentum. Specifically, through the study of the Lamb vector, its divergence and its transport, we explore the broader question of whether specific field variables that conform to these requirements are able to provide a rigorous foundation for identifying and studying those motions that carry the bulk of the dynamics. Of course, such concepts are not entirely new. For example, some researchers have

suggested that coherent motions might be mathematically connected to the field variable of helicity (Tsinober & Levich 1983; Moffatt 1985). Similarly, Klewicki (1998) hypothesized, on physical grounds, a direct connection between the mechanisms underlying coherent motion formation and evolution, and turbulent stress transport. The primary hypothesis investigated herein relates to the Lamb vector divergence as a derived field variable that intrinsically identifies those spatially localized motions having a distinct capacity to effect a time rate of change of momentum (i.e. to a degree that is disproportionate with the volume it occupies) and, thus, contains both desirable attributes asserted above.

Given these considerations, the objectives of the present study are to

(i) describe the mathematical and physical properties of the Lamb vector divergence that establish its relation to those motions that effect a time rate of change of linear momentum,

(ii) elucidate the generic characteristics of the Lamb vector divergence by exploring its behaviour in representative analytical test problems, and

(iii) explore the behaviour of the Lamb vector divergence in a range of complex flows (both turbulent and unsteady) relative to its capacity to identify the dynamically important motions.

Given these objectives, it is useful to briefly discuss previous research concerning the Lamb vector and its derivatives. Wu, Ma & Zhou (2006) analysed the Lamb vector for a wide variety of flows including slender-wing drag reduction (Yang *et al.* 2007). Moffatt (1985, 1986*a*,*b*) investigated the Lamb vector in the context of steady Euler flow and magnetohydrodynamic equilibria. The Lamb vector divergence appears in the equations of Marmanis (1998) as a source term. Sposito (1997) and Kollmann (2006) analysed Lamb surfaces and vector fields. Tsinober (1990) studied the relationship between the Lamb vector and the depression of non-linearity in turbulent flows. Rousseaux *et al.* (2007) and Alim (2007) have both measured the Lamb vector divergence experimentally by PIV. The Lamb vector divergence also appears as an acoustic source term in Lighthill's wave equation (Lighthill 1952) and, more directly, in the formulation of Howe (1975). In this context, the interaction between adjacent high- and low-momentum (or pressure) fluid parcels associated with compression (or sound) waves is given new clarity by the interpretation of the Lamb vector divergence outlined in the following sections.

In § 2, we describe several mathematical properties and physical interpretations of the Lamb vector divergence that substantiate its kinematical and dynamical significance. The equations of motion are reviewed in § 3 in order to derive a transport equation for the Lamb vector divergence and formulate a transport-equation-based methodology for the study of coherent motions. Analytic examples of shear flow, vortex flow, and chaotic Beltrami flow fields are then used to clarify these properties in § 4. The statistical and instantaneous properties of the Lamb vector divergence for a variety of topologically complex flow fields are analysed in § 5 to illustrate the dynamical importance of the Lamb vector divergence. The present results are then summarized and discussed in § 6.

2. Mathematical and physical properties

The Lamb vector divergence can be expressed as the sum of two parts: (1) the flexion product $\boldsymbol{u}\cdot\nabla\times\boldsymbol{\omega}$ and (2) the negative enstrophy $-\boldsymbol{\omega}\cdot\boldsymbol{\omega}$,

$$\nabla\cdot\boldsymbol{l} = \boldsymbol{u}\cdot\nabla\times\boldsymbol{\omega} - \boldsymbol{\omega}\cdot\boldsymbol{\omega}\ , \tag{2.1}$$

where $\boldsymbol{l} = \boldsymbol{\omega} \times \boldsymbol{u} = (\nabla \times \boldsymbol{u}) \times \boldsymbol{u}$ is the vorticity–velocity cross-product, or Lamb vector. Accordingly, the Lamb vector divergence is identically zero for both irrotational and Beltrami flows where $\boldsymbol{\omega} \times \boldsymbol{u} = 0$, or more generally, whenever the Lamb vector is solenoidal. The flexion product and enstrophy, however, need not be zero if the Lamb vector divergence is zero. In such a case, the flexion product and enstrophy are locally balanced, i.e. $\boldsymbol{u} \cdot \nabla \times \boldsymbol{\omega} = \boldsymbol{\omega} \cdot \boldsymbol{\omega}$. Such regions where the sign of the Lamb vector divergence switches between negative and positive occur frequently in turbulent flows. When this shift occurs, the mechanisms that drive momentum transfer in turbulent flows undergo a distinct change in dynamical character.

Equation (2.1) indicates that, for any vortical flow, the last term will always be negative. Negative values of $\nabla \cdot \boldsymbol{l}$ are interpreted as spatially localized motions that have accumulated the capacity to effect a time rate of change of linear momentum. Conversely, spatially localized positive regions represent motions that have a depleted capacity in this regard. Relative to the generic notion of a vortex mentioned in the Introduction, it is tempting to associate the former of these attributes with the concentrated angular momentum in a swirling-type motion. This interpretation does not, however, require a vortex-like motion since a shear layer embedded in a turbulent flow can just as easily generate locally large amplitude enstrophy fluctuations. On the other hand, while the overall Lamb vector divergence can be either positive or negative, positive contributions can only arise owing to the flexion product. Since $\boldsymbol{u} \cdot \nabla \times \boldsymbol{\omega} = -\boldsymbol{u} \cdot \nabla^2 \boldsymbol{u}$ for isochoric motions, $\boldsymbol{u} \cdot \nabla^2 \boldsymbol{u}$ is negative when the flexion product is positive. Physical processes associated with such motions would seem to be the unwinding of a vortex: the conversion of the angular momentum stored in a rotational motion into linear momentum and the depletion of the low-pressure zone (owing to the Euler-n effect) associated with a vortex core. Since the Lamb vector divergence is parity invariant, the interpretations given for both positive and negative regions of Lamb vector divergence are independent of whether or not one uses a right- or left-handed frame of reference (Moffatt & Tsinober 1992).

Application of Green's transformation in any volume of fluid V yields

$$\int_V (\nabla \cdot \boldsymbol{l}) \, \mathrm{d}V = \int_V (\boldsymbol{u} \cdot \nabla \times \boldsymbol{\omega} - \boldsymbol{\omega} \cdot \boldsymbol{\omega}) \, \mathrm{d}V = \oint_S (\boldsymbol{\omega} \times \boldsymbol{u}) \cdot \mathrm{d}\boldsymbol{S}, \tag{2.2}$$

where it is understood that the unit normal $\mathrm{d}\boldsymbol{S}$ points outward from the bounding surface of integration S. As is always the case, the total divergence of the Lamb vector in a region equals the net outward flux of the Lamb vector across the boundary of that region. Recognizing that the Lamb vector acts as a vortex force, the Lamb vector divergence identifies inhomogeneities in the momentum transport surrounding a fluid element, or a flux of energy, that propagates or concentrates local energy curvature. In a region of flow where the flexion product is positive, the enstrophy acts as a storage mechanism and the flexion product behaves like a release mechanism of the momentum flux and kinetic energy as shown in § 5. The total Lamb vector divergence in a given region is then given by the sum of all sources (i.e. flexion product) minus the sum of all sinks (i.e. enstrophy) of force gradients. For a wide variety of flows, e.g. shear layers and vortex flows, the flexion product is positive so that the aforementioned source–sink interpretation is appropriate. Furthermore, the mutual interference between the flexion product and enstrophy gives rise to an energy curvature interpretation and minimization process for flow interactions outlined in the following sections.

2.1. *The Lamb vector divergence and the Bernoulli function*

The convective acceleration of a material particle can be written as the sum of the Lamb vector and the gradient of the specific kinetic energy: $(\boldsymbol{u}\cdot\nabla)\boldsymbol{u}=\boldsymbol{\omega}\times\boldsymbol{u}+\nabla(u^2/2)$. The mathematical and physical character of the Lamb vector plays an important role in establishing the nature of the flow (Truesdell 1954), and ∇u^2 describes how material particles accelerate as they move towards kinetic energy maxima. Well known bounds for isochoric flows show that $-\boldsymbol{\omega}\cdot\boldsymbol{\omega}/2\leqslant\nabla\cdot[(\boldsymbol{u}\cdot\nabla)\boldsymbol{u}]\leqslant\boldsymbol{S}^2$ where $\boldsymbol{S}$ is the rate of strain tensor $S_{ij}=(u_{i,j}+u_{j,i})/2$ and $\boldsymbol{S}^2=S_{ij}S_{ji}$ is non-negative. By rearranging terms,

$$\tfrac{1}{2}\boldsymbol{\omega}\cdot\boldsymbol{\omega}\leqslant\boldsymbol{u}\cdot\nabla\times\boldsymbol{\omega}+\nabla^2\left(\tfrac{1}{2}u^2\right)\leqslant\boldsymbol{S}^2+\boldsymbol{\omega}\cdot\boldsymbol{\omega}, \tag{2.3}$$

so that the middle expression must be non-negative for all isochoric motions. Then, if the squared speed is superharmonic (i.e. $\nabla^2u^2<0$) on some connected open subset M of the flow domain, the flexion product is necessarily positive throughout M and, by the properties of superharmonic functions, the least value of u^2 is attained on the boundary ∂M. Therefore, if the kinetic energy obtains a local maximum at a point P, then there exists a region M containing P where the squared speed is superharmonic.

In such a case, we have a 'pocket' of high-speed fluid surrounded by low-speed fluid. The natural question to then ask is what happens to this high-energy content fluid? The flow seeks to minimize this energy (or momentum flux) curvature by redistributing its momentum to the surrounding low-speed fluid. Positive flexion product is seen to identify this momentum transfer process. Furthermore, the appearance of the flexion product in the viscous contribution to the kinetic energy transport equation (see § 3) results in the interpretation that $\boldsymbol{u}\cdot\nabla\times\boldsymbol{\omega}$ is primarily positive so as to decrease the local fluid velocity through viscous effects. Hence, the flexion product is also characteristic of kinetic energy dissipation supporting the aforementioned energy minimization process. For isochoric motions, the flexion product can be expressed as

$$\boldsymbol{u}\cdot\nabla\times\boldsymbol{\omega}=\boldsymbol{S}^2+(\boldsymbol{\omega}\cdot\boldsymbol{\omega}-\nabla^2u^2)/2, \tag{2.4}$$

where positive flexion product is also readily explainable in terms of the harmonic behaviour of the momentum flux and subsequent temporal interactions between adjacent regions of such variation.

Equations (2.3) and (2.4) do not, however, prohibit negative flexion product. If the flexion product is negative throughout a connected region G, then the squared speed is necessarily subharmonic (i.e. $\nabla^2u^2>0$) throughout G, and hence the greatest u^2 must be found on the boundary ∂G. Therefore, we now have a pocket of low-speed fluid surrounded by high-speed fluid. This is characteristic of regions of separated flow where the flexion product is negative, as seen in the turbulent cylinder flow of § 5.2. Equation (2.4) also suggests that positive flexion product can be found where the squared speed is subharmonic, e.g. in the predominantly low-speed high-vorticity environment of the viscous sublayer. From (2.3), the harmonic nature of u^2 becomes indefinite in regions where $-\boldsymbol{\omega}\cdot\boldsymbol{\omega}/2<\nabla\cdot\boldsymbol{l}<\boldsymbol{S}^2$, e.g. at the interface between the viscous sublayer and buffer layer in turbulent channel flow as shown in § 5.1. In such regions, the Lamb vector divergence and energy curvature relationship is further clarified by the dynamical interpretation afforded by the momentum flux plus pressure, or Bernoulli function.

Taking the divergence of the momentum equation yields that $\nabla\cdot\boldsymbol{l}=-\nabla^2(\phi^*+u^2/2)$ for isochoric motions where ϕ^* is the acceleration potential given by $\phi^*=p/\rho$ for an incompressible Navier–Stokes flow with pressure p and density ρ. The form of these equations suggests defining a new scalar potential $\Phi=\phi^*+u^2/2$, which is known

as the Bernoulli function. Therefore, for a Navier–Stokes flow, the Lamb vector divergence is the source term in a Poisson equation for the Bernoulli function:

$$\nabla \cdot \boldsymbol{l} = -\nabla^2 \left(\frac{p}{\rho} + \frac{u^2}{2} \right) = -\nabla^2 \Phi. \tag{2.5}$$

Hence, for a given region of flow, if $\nabla \cdot \boldsymbol{l} \geqslant 0$, it follows that Φ is superharmonic so that the least value of Φ occurs on the boundary indicative of a local maximum of Bernoulli function. If $\nabla \cdot \boldsymbol{l} \leqslant 0$, then Φ is subharmonic so that the maximum value of Φ occurs on the boundary indicative of a local minimum of Bernoulli function. Furthermore, if $\nabla \cdot \boldsymbol{l} = 0$, then no local maxima or minima occur in the interior. Therefore, regions of positive $\nabla \cdot \boldsymbol{l}$ physically correspond to regions where Φ is concentrated, while regions of negative $\nabla \cdot \boldsymbol{l}$ correspond to regions where Φ is depleted.

Positive values of Lamb vector divergence represent straining motions owing to the flexion product, while negative values represent vorticity bearing motions. As a result, straining motions constitute a local concentration of flow energy, while non-straining vortical motions represent a locally depleted region of flow energy. More importantly, however, the interaction and interference between regions of strong strain rate and regions of strong vorticity carries a strong potential relative to the surrounding fluid to redistribute this energy thereby converting low-speed high-vorticity motions into high-speed low-vorticity motions (and vice versa) as described by the Lamb vector divergence. These local energy variations and their subsequent temporal interactions possess a significant potential relative to the surroundings to redistribute momentum, thereby effecting a time rate of change of momentum through the dynamical processes discussed in § 3.

2.2. *Pressure drag*

Of particular interest is the relationship between the Lamb vector divergence and the drag (or lift) on a stationary bluff body immersed in an incompressible flow. The resultant force $\boldsymbol{F}_{\text{net}}$ due to pressure is then given by integration of the general solution of (2.5) along the surface S_0 of the bluff body

$$\boldsymbol{F}_{\text{net}} = -\frac{\rho}{4\pi} \int_V \nabla \cdot \boldsymbol{l}(\boldsymbol{r}') \oint_{S_0} \frac{1}{|\boldsymbol{r}' - \boldsymbol{r}|} \, \mathrm{d}\boldsymbol{S}(\boldsymbol{r}) \, \mathrm{d}V(\boldsymbol{r}'), \tag{2.6}$$

where the spatial distribution of the Lamb vector divergence and geometry are the critical parameters. Observe that, when the Lamb vector divergence is zero, the contribution to the net force is identically zero. Moreover, if one can minimize or balance the spatial distribution of the flexion product and enstrophy, the drag will decrease significantly.

For example, decreasing the area over which regions of positive and negative Lamb vector divergence interact leads to drag reduction, which is exactly what happens, for example, when increasing the Reynolds number in cylinder flows as shown in § 5. The drag can also be reduced by balancing the spatial distribution of the Lamb vector divergence through injection of high-momentum fluid into regions where the flexion product is dominant. A similar process is observed in the case of bubble injection into a turbulent boundary layer. In this case, the bubbles act to flatten the energy curvature. This produces a more harmonic Bernoulli function relative to the non-bubble case and, as a result, reduces the net viscous drag (Xu, Maxey & Karniadakis 2002; Ferrante & Elghobashi 2004). A cylinder subject to rotary oscillation (Shiels & Leonard 2001; Protas & Wesfreid 2001) also experiences drag

reduction, as evident from (2.6), due to the increased strength of near-wall enstrophy. Geometry modifications also impact the Lamb vector divergence distribution, e.g. streamwise riblets form a barrier of positive Lamb vector divergence that prevents deceleration of high-speed fluid at the wall surface, thereby reducing the drag (Choi, Moin & Kim 1993).

Investigating these effects of the Lamb vector divergence in the context of drag reduction provides a valuable analysis tool for a wide variety of complex flows (Crawford, Marmanis & Karniadakis 1998). Such analysis is further aided by recognizing that, like the vorticity, the distribution of the Lamb vector divergence can be inferred for a given geometry, thereby enabling the development of drag reduction methodologies in conjunction with (2.6) by inspection alone. The problem of drag reduction has effectively been reduced to an integral minimization problem whereby balancing the Lamb vector divergence, or equivalently, harmonizing the Bernoulli function will decrease the drag.

2.3. *Integral properties*

A well-known identity of Lamb and J. J. Thomson (Truesdell 1951) when expressed in terms of the Lamb vector divergence reveals that

$$\frac{1}{2}\int_V u^2 \,\mathrm{d}V = \oint_S \left[\frac{1}{2}u^2\boldsymbol{r} - (\boldsymbol{u}\cdot\boldsymbol{r})\boldsymbol{u} + \frac{r^2}{2}\boldsymbol{l}\right]\cdot \mathrm{d}\boldsymbol{S} - \frac{1}{2}\int_V r^2 \nabla\cdot\boldsymbol{l}\,\mathrm{d}V, \tag{2.7}$$

provided that $\boldsymbol{u}$ is solenoidal. Therefore, the total kinetic energy of the flow is directly related to a weighted volume integral of the Lamb vector divergence. For a bluff body, contributions from the geometry are decoupled from the local dynamics near the wall of the body, which becomes more clearly defined with increasing Reynolds number due to the increasing spatial localization of the Lamb vector divergence. This decoupling effect appears to be a rather generic feature of the Lamb vector divergence.

From (2.2), if all finite boundaries are no-slip and stationary, it is sufficient that $\boldsymbol{l}\cdot\boldsymbol{n}$ decay as fast as r^{-2} in the far field so that

$$\int_V \nabla\cdot\boldsymbol{l}\,\mathrm{d}V = 0. \tag{2.8}$$

This implies that the average value of the Lamb vector divergence is zero over the entire motion independent of whether or not that motion is isochoric. Hence, for a wide class of motions, the Bernoulli function is harmonic on average (e.g. the vortex flow of § 4.2). This implies a global balance between the flexion product and enstrophy – albeit not necessarily a local balance except for the trivial case of rest. Therefore, on average, turbulent flows seek to minimize the energy curvature, or equivalently, harmonize the Bernoulli function. The process by which this occurs find rigorous description via the self-interaction of competing positive and negative Lamb vector divergence regions. As shown later, the formation and evolution of these local variations in the Lamb vector divergence constitute a predominant characteristic of turbulent flows.

3. Transport

In this section, the transport equation for the Lamb vector divergence is examined. The motivation behind this development is to understand the physical mechanisms

that drive the Lamb vector divergence and to provide new insight into coherent motion development and evolution that is not otherwise apparent. We now consider the special forms of the general transport equations for Newtonian fluids.

The transport equation for the Lamb vector divergence is

$$\frac{\partial(\nabla\cdot\boldsymbol{l})}{\partial t}=(\nabla\times\boldsymbol{\omega})\cdot\frac{\partial\boldsymbol{u}}{\partial t}+\boldsymbol{u}\cdot\frac{\partial(\nabla\times\boldsymbol{\omega})}{\partial t}-2\boldsymbol{\omega}\cdot\frac{\partial\boldsymbol{\omega}}{\partial t}, \tag{3.1}$$

where the first two terms represent the flexion product transport equation and the last embodies the enstrophy transport equation. We now analyse each term.

The momentum transport equation is

$$\frac{\partial\boldsymbol{u}}{\partial t}+\boldsymbol{l}=-\nabla\Phi-\nu\nabla\times\boldsymbol{\omega}, \tag{3.2}$$

where ν is the kinematic viscosity. Similarly, the kinetic energy transport equation is

$$\frac{1}{2}\frac{\partial u^2}{\partial t}=-\boldsymbol{u}\cdot\nabla\Phi-\nu\boldsymbol{u}\cdot(\nabla\times\boldsymbol{\omega}), \tag{3.3}$$

where the flexion product appears as a dissipative mechanism. Since the kinetic energy is a non-negative quantity, this further provides evidence that the flexion product term is primarily positive in non-separated flow regions as the viscous contributions would be expected to decrease the total kinetic energy. If the motion is steady, the Bernoulli function also decreases along the flow direction when the flexion product is positive as expected of a straining motion (Batchelor 1967).

One may write the enstrophy transport equation as

$$\boldsymbol{\omega}\cdot\frac{\partial\boldsymbol{\omega}}{\partial t}=-\boldsymbol{\omega}\cdot\nabla\times\boldsymbol{l}+\nu\boldsymbol{\omega}\cdot\nabla^2\boldsymbol{\omega}, \tag{3.4}$$

where the curl of the Lamb vector contributes to the advection and stretching of vorticity. In a manner analogous to that of the kinetic energy transport equation, $\boldsymbol{\omega}\cdot\nabla^2\boldsymbol{\omega}$ is primarily negative so as to decrease the enstrophy through viscous action. Therefore, the primary mechanism to produce an increase in enstrophy results from negative $\boldsymbol{\omega}\cdot\nabla\times\boldsymbol{l}$. Note that this term is also negative for similar vorticity filament topologies in a steady vorticity field, i.e. $\boldsymbol{\omega}\cdot\nabla\times\boldsymbol{l}=\nu\boldsymbol{\omega}\cdot\nabla^2\boldsymbol{\omega}$. Hence, $\boldsymbol{\omega}\cdot\nabla\times\boldsymbol{l}$ is typically negative when the enstrophy is increasing. However, after the enstrophy has reached a local maximum and begins to decrease, these terms reverse their roles.

Applying the curl operator twice to (3.2) yields the transport equation for the flexion whose dot product with the velocity field yields

$$\boldsymbol{u}\cdot\frac{\partial(\nabla\times\boldsymbol{\omega})}{\partial t}=-\boldsymbol{u}\cdot\nabla(\nabla\cdot\boldsymbol{l})+\boldsymbol{u}\cdot\nabla^2\boldsymbol{l}+\nu\boldsymbol{u}\cdot\nabla^2(\nabla\times\boldsymbol{\omega}), \tag{3.5}$$

where $\boldsymbol{u}\cdot\nabla(\nabla\cdot\boldsymbol{l})$ is the advection of the Lamb vector divergence. The biharmonic term $\boldsymbol{u}\cdot\nabla^2(\nabla\times\boldsymbol{\omega})=-\boldsymbol{u}\cdot\nabla^4\boldsymbol{u}$ is typically negative along a streamline in a region of positive Lamb vector divergence where ∇^2u^2 is increasing as the fluid particle transmits its kinetic energy and momentum flux to the surrounding fluid. This term then acts to minimize a further increase in flexion product, or momentum, through viscous effects as the surrounding low-momentum fluid is accelerated. Correspondingly, in regions of negative Lamb vector divergence where ∇^2u^2 is decreasing, this term is primarily positive, effectively promoting a more harmonic Bernoulli function as described below.

By substituting (3.2), (3.4) and (3.5) into (3.1), the Lamb vector divergence transport equation takes the form

$$\frac{\mathrm{D}(\nabla\cdot\boldsymbol{l})}{\mathrm{D}t} = \boldsymbol{u}\cdot\nabla^2\boldsymbol{l} + 2\boldsymbol{\omega}\cdot(\nabla\times\boldsymbol{l}) + \boldsymbol{l}\cdot\nabla^2\boldsymbol{u} - (\nabla\times\boldsymbol{\omega})\cdot\nabla\Phi + \nu[-(\nabla\times\boldsymbol{\omega})^2 + \boldsymbol{u}\cdot\nabla^2(\nabla\times\boldsymbol{\omega}) - 2\boldsymbol{\omega}\cdot\nabla^2\boldsymbol{\omega}], \quad (3.6)$$

where each term has dimensions of energy flux. Observe that the viscous terms owing to the flexion product, specifically $-(\nabla\times\boldsymbol{\omega})^2$ and $\boldsymbol{u}\cdot\nabla^2(\nabla\times\boldsymbol{\omega})$, are typically negative where $\nabla\cdot\boldsymbol{l}>0$, while the enstrophy term $-2\boldsymbol{\omega}\cdot\nabla^2\boldsymbol{\omega}$ is typically positive where $\nabla\cdot\boldsymbol{l}<0$. Physically, this means that regions of strong flexion product tend to locally decrease the flexion product throughout the flow while regions with strong enstrophy tend to locally decrease the enstrophy thereby collectively minimizing the Bernoulli function towards a harmonic state through the action of viscosity. A similar action of harmonic minimization occurs for the flexion product terms in regions of strong enstrophy and for the enstrophy terms in regions of strong flexion product. One mechanism by which viscous effects minimize $\nabla^2\Phi$ is through enhanced alignment of the vorticity and velocity vectors. In effect, viscous processes act to return the flow to a harmonic state while the extra advective terms act to make the Lamb vector divergence depart from equilibrium. This latter effect leads to more intense momentum and energy transfer.

Recalling that the velocity and flexion vectors must be correlated for the flexion product to be positive, $(\nabla\times\boldsymbol{\omega})\cdot\nabla\Phi$ is generally of the same sign as $\boldsymbol{u}\cdot\nabla\Phi$. Therefore, the term $-(\nabla\times\boldsymbol{\omega})\cdot\nabla\Phi$ is expected to be primarily positive in regions of strongly positive flexion product. In such cases, the Bernoulli function decreases in the flow direction. Such streamline behaviour is common even in unsteady, inviscid flows where a local maximum in kinetic energy subsequently decreases in time by the transport of momentum flux curvature to the surrounding fluid as $\boldsymbol{u}\cdot\nabla\Phi=-\partial_t(u^2/2)$. Therefore, this term is interpreted to measure how a region of high-flexion product expends its kinetic energy and increases its pressure, which then increases the momentum and decreases the pressure of the surrounding fluid.

The remaining advective terms act to enhance the magnitude of the flexion product and enstrophy, correspondingly. By definition, the Lamb vector is orthogonal to the velocity, and hence, $\boldsymbol{l}\cdot\nabla^2\boldsymbol{u}$ is seen to characterize the transport of momentum flux curvature to the surrounding fluid in the plane perpendicular to the velocity vector. For steady flow, $\nu\boldsymbol{l}\cdot\nabla^2\boldsymbol{u}=l^2+\boldsymbol{l}\cdot\nabla\Phi$. Therefore, $\boldsymbol{l}\cdot\nabla^2\boldsymbol{u}$ is primarily positive in a region where the momentum flux is increasing perpendicular to the velocity field, while it is negative where the momentum flux is decreasing orthogonally to the velocity field. Hence, $\boldsymbol{l}\cdot\nabla^2\boldsymbol{u}$ is typically positive where low-momentum fluid is being accelerated.

Similarly, $\boldsymbol{u}\cdot\nabla^2\boldsymbol{l}$ appears due to the flexion product transport equation and is expected to be positive in a region of increasing Lamb vector divergence (e.g. where the fluid is accelerating). Likewise, $\boldsymbol{u}\cdot\nabla^2\boldsymbol{l}$ is typically negative in a region of decreasing Lamb vector divergence (e.g. where the fluid is decelerating). This term then measures the transport of momentum flux curvature to the surrounding fluid. This occurs along a streamline as the flow evolves from a low-momentum flux to a high-momentum flux condition, and leads to an increase in linear momentum that is subsequently attenuated by the surrounding low-momentum fluid. This interpretation is clarified by recognizing that, for steady inviscid flow, $\boldsymbol{u}\cdot\nabla^2\boldsymbol{l}=-\boldsymbol{u}\cdot\nabla(\nabla^2\Phi)=\boldsymbol{u}\cdot\nabla(\nabla\cdot\boldsymbol{l})$, which remains a dominant contribution for unsteady viscous flow. Thus, if the Bernoulli function is decreasing along a streamline, the magnitude of its curvature is minimized in the flow direction such that $\boldsymbol{u}\cdot\nabla^2\boldsymbol{l}$ is negative. This will occur, for example, in a region immediately following a local maximum of flexion product and Lamb vector divergence, where the net viscous force acts to decelerate the fluid. This reflects

how viscous effects act to harmonize the Bernoulli function along the flow direction. Analogously, $\boldsymbol{u}\cdot\nabla^2\boldsymbol{l}$ is typically positive in regions immediately following a local maximum of enstrophy in subharmonic regions.

Equation (3.4) indicates that $\boldsymbol{\omega}\cdot(\nabla\times\boldsymbol{l})$ is typically negative in regions where the enstrophy is increasing and positive in regions where the enstrophy is decreasing. Therefore, this term acts to locally concentrate angular momentum in regions where there is a deficit of linear momentum and redistribute regions of high enstrophy. These regions of momentum deficit then lead to a superharmonic state in part as a result of this initial enstrophy concentration, which has an increased capacity to effect a time rate of change of momentum. The flexion product advection terms represent the mechanisms by which this capacity is activated and, in the case of a localized low-momentum region, dictate the interaction with the surrounding high-momentum fluid.

An interesting reformulation of these extra advective terms follows from the kinematically exact result that

$$\boldsymbol{u}\cdot\nabla^2\boldsymbol{l}+2\boldsymbol{\omega}\cdot\nabla\times\boldsymbol{l}+\boldsymbol{l}\cdot\nabla^2\boldsymbol{u}=-2(\nabla\boldsymbol{u}):(\nabla\boldsymbol{l}), \tag{3.7}$$

where $(\nabla\boldsymbol{u}):(\nabla\boldsymbol{l})=(\partial_i u_j)(\partial_j l_i)$ denotes the double contraction of the velocity gradient tensor and the Lamb vector gradient tensor. Hence, the Lamb vector divergence transport equation may be rewritten as

$$\frac{\mathrm{D}(\nabla\cdot\boldsymbol{l})}{\mathrm{D}t}=-2(\nabla\boldsymbol{u}):(\nabla\boldsymbol{l})-(\nabla\times\boldsymbol{\omega})\cdot\nabla\Phi+\nu[-(\nabla\times\boldsymbol{\omega})^2+\boldsymbol{u}\cdot\nabla^2(\nabla\times\boldsymbol{\omega})-2\boldsymbol{\omega}\cdot\nabla^2\boldsymbol{\omega}]. \tag{3.8}$$

This form reveals that the non-orthogonality or coalignment between the velocity and Lamb vector gradients is a generic feature associated with the production and transport of the Lamb vector divergence, and consequentially drives the mixing of momentum and energy throughout the flow.

In this section, we have shown how the terms that appear in the transport equation for the Lamb vector divergence are associated with the flexion product and enstrophy transport. The viscous terms act to attenuate the momentum flux curvature and promote a harmonic balance, often through alignment of the vorticity and velocity vectors. Conversely, the advective terms push the Lamb vector divergence away from equilibrium. Specifically, the flexion product terms act to increase the kinetic energy in subharmonic regions leading to a superharmonic state. In contrast, the advective enstrophy transport terms act to increase the enstrophy magnitude in superharmonic regions, thereby promoting a subharmonic state. The terms in (3.6) delineate how the Lamb vector divergence identifies motions in the flow that have a distinct capacity to transport, mix, and redistribute energy and momentum.

Given the actions induced from either the subharmonic or superharmonic condition, the tendency is for the above processes to repeat, i.e. initially low-momentum subharmonic fluid parcels store momentum flux capacity from the surrounding high-momentum fluid due to the advective enstrophy terms, and subsequently activate this capacity via interactions described by the advective flexion product terms. These mechanisms provide considerable insight into what spatially localized motions have the greatest capacity to effect a time rate of change of momentum. Perhaps not surprisingly, the regenerative nature of these mechanisms is also a generic property of the self-sustaining dynamical processes attributed to coherent motions in turbulent flows.

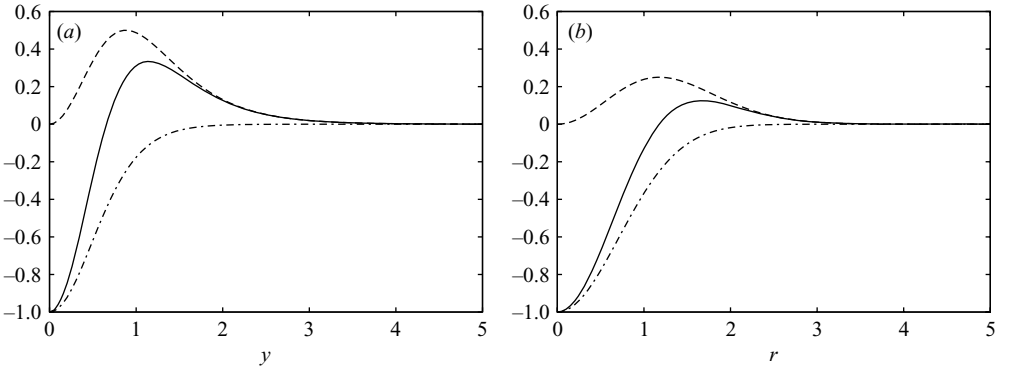

FIGURE 1. Flexion product (dash), enstrophy (dash–dot), and Lamb vector divergence (solid) profiles for (*a*) unidirectional shear flow and (*b*) Burgers' vortex scaled by core enstrophy.

4. Analytical examples

For the purposes of revealing generic properties of the Lamb vector divergence, it is instructive to examine a select set of analytical examples.

4.1. *Shear flow*

For a unidirectional shear flow with $\boldsymbol{u} = (U(y,t), 0, 0)^T$, we have that

$$\nabla\cdot\boldsymbol{l} = -U\frac{\partial^2 U}{\partial y^2} - \left(\frac{\partial U}{\partial y}\right)^2, \tag{4.1}$$

where the first term is the flexion product and the second term the enstrophy. Let, for example, the steady velocity profile be given by $U(y) = \tanh(y)$, where y is the non-dimensional distance normalized by an appropriate length scale, e.g. the shear layer thickness. As shown in figure 1, the distribution of the non-dimensional Lamb vector divergence for this particular velocity profile is

$$\nabla\cdot\boldsymbol{l} = -(1-\tanh^2(y))(1-3\tanh^2(y)). \tag{4.2}$$

The Lamb vector divergence reaches a global minimum at the origin. It then passes through zero, where the flexion product and enstrophy balance, and reaches a maximum shortly thereafter. Since the vorticity decreases monotonically with increasing distance from the origin (wall), the flexion product is non-negative.

Equation (2.3) indicates that the kinetic energy is subharmonic where $\nabla\cdot\boldsymbol{l} \leqslant -\boldsymbol{\omega}\cdot\boldsymbol{\omega}/2$ (i.e. $y \leqslant 0.48$) and superharmonic for $\nabla\cdot\boldsymbol{l} \geqslant \boldsymbol{S}^2$ (i.e. $y \geqslant 0.78$). By inspection of (2.3) alone, however, the harmonic state of the kinetic energy is indefinite where the Lamb vector divergence transitions from negative to positive near $y = 0.66$, specifically, in the region where $-\boldsymbol{\omega}\cdot\boldsymbol{\omega}/2 < \nabla\cdot\boldsymbol{l} < \boldsymbol{S}^2$. This region is similar to the region where the viscous sublayer transitions to the buffer layer in turbulent boundary layers as discussed in § 5.1. Since, however, the convective acceleration is zero in this flow, the Lamb vector is completely determined by its potential part such that $\nabla\cdot\boldsymbol{l} = -\nabla^2 u^2/2$ with $\nabla^2 p = 0$. Hence, the kinetic energy (like the Bernoulli function) is subharmonic wherever $\nabla\cdot\boldsymbol{l} \leqslant 0$ and superharmonic wherever $\nabla\cdot\boldsymbol{l} \geqslant 0$ for unidirectional shear flow. As shown in § 5, the interaction between negative and positive regions of Lamb vector divergence, like those shown in figure 1, is a key characteristic of many complex flows.

4.2. *Vortex flow*

For a steady Burgers vortex with vortex Reynolds number $1/A$ (see e.g. Marcu, Meiburg & Newton 1994), the non-dimensional Lamb vector divergence is

$$\nabla\cdot\boldsymbol{l} = \left(\frac{-1}{4\pi^2}\right)\left[2\exp\left(-r^2\right) - \exp\left(\frac{-r^2}{2}\right)\right], \tag{4.3}$$

as shown in figure 1. These distributions are qualitatively similar to the unidirectional shear flow of § 4.1 despite their quantitative differences. In particular, $\nabla^2 p$ is not zero in this three-dimensional vortex flow, which guarantees a well-defined transition region, in contrast to planar shear flow. For vortex flows, the Lamb vector divergence identifies the inhomogeneity between the local concentration of enstrophy at the core and the surrounding dissipative mechanisms driven by the flexion product.

The Lamb vector divergence is invariant with respect to the vortex Reynolds number when normalized as shown and, thus, is independent of the background straining motion. Comparison with (2.3) reveals that $\nabla^2 u^2$, $\nabla^2 p$, and $\boldsymbol{S}^2$ are not invariant with respect to the vortex Reynolds number, and furthermore, are all unbounded in the radial and axial directions for any finite Reynolds number. However, the enstrophy, flexion product, and Lamb vector divergence all remain bounded and invariant.

The physical reason for this behaviour is found from the vortex pressure distribution

$$p(r,z) = p_0 + \int_0^r \frac{[u_\theta(r')]^2}{r'}\,\mathrm{d}r' - A^2(r^2/2 + 2z^2), \tag{4.4}$$

where p_0 is an arbitrary constant. Observe that $u^2/2 = u_\theta^2/2 + A^2(r^2/2 + 2z^2)$. Then, to within an arbitrary constant, the Bernoulli function $\Phi(r) = p + u^2/2$ is given by

$$\Phi(r) = \frac{1}{8\pi^2}[\mathrm{Ei}(r^2) - \mathrm{Ei}(r^2/2)], \tag{4.5}$$

where $\mathrm{Ei}(x)$ is the exponential integral. Therefore, the pressure balances the momentum flux in the limit as $r \to \infty$. This result is independent of the vortex Reynolds number such that the Bernoulli function remains bounded and only radially dependent even though both the pressure and squared speed individually diverge in the radial and axial directions. Vortex and shear flows exhibit dynamic similarity between strain rate and vorticity interactions. This directly follows from the interference between the flexion product and enstrophy. This interference is characterized by an energy sink at the vortex core (or wall) followed closely by a strong shift to an attenuated energy source.

4.3. *ABC flow*

For an Arnold–Beltrami–Childress (ABC) flow (Dombre *et al.* 1986),

$$\boldsymbol{u} = (A\sin z + C\cos y,\ \ B\sin x + A\cos z,\ \ C\sin y + B\cos x),$$

where A, B, and C are constant parameters. This type of flow is characterized by regions of concentrated vorticity with non-zero helicity (i.e. $\boldsymbol{u}\cdot\boldsymbol{\omega} \neq 0$). ABC flows are solutions of the steady Euler equation as well as an unsteady, forced Navier–Stokes equation. For particular parameter values, ABC flows are also known to exhibit chaotic particles paths. However, since ABC flow is a Beltrami flow where $\boldsymbol{\omega} = \lambda\boldsymbol{u}$ with λ constant, the Lamb vector divergence and the Lamb vector are both identically zero as the vorticity and velocity are parallel throughout the flow domain. The enstrophy is, however, non-zero, and hence, $\boldsymbol{u}\cdot\nabla\times\boldsymbol{\omega} = \boldsymbol{\omega}\cdot\boldsymbol{\omega}$. Therefore, in a Beltrami flow, the flexion product (or local kinetic energy dissipation) is exactly balanced

by the enstrophy. For a Beltrami flow with uniform Bernoulli function, the viscous terms in the Lamb vector divergence transport equation sum to zero since $\boldsymbol{\omega}\cdot\nabla^2\boldsymbol{\omega} = -(\nabla\times\boldsymbol{\omega})^2 = \boldsymbol{u}\cdot\nabla^2(\nabla\times\boldsymbol{\omega})$. Therefore, $\boldsymbol{\omega}\cdot\nabla^2\boldsymbol{\omega} = \boldsymbol{u}\cdot\nabla^2(\nabla\times\boldsymbol{\omega}) \leqslant 0$ in agreement with the analysis of § 3.

ABC flows and, more generally, Beltrami flows are often associated with both vortical and turbulent motions, e.g. Moffatt & Tsinober (1992). Vorticity is not, however, advected or stretched in a Beltrami flow. One further observes that, if the Lamb vector divergence is identically zero in an isochoric Newtonian fluid, the Bernoulli function is harmonic and therefore cannot have local maxima or minima. As a result, the periodicity and continuity of an ABC flow dictate that the Bernoulli function, or stagnation pressure p_0, is uniformly constant throughout the domain such that $|\boldsymbol{u}| = \sqrt{2(p_0 - p)/\rho}$. Furthermore, steady ABC flow is circulation-preserving. These dynamically uninteresting properties draw into question the usefulness of ABC flow and Beltrami motions in the study of material-based formulations and vortex identification schemes. This flow explicitly lacks the qualities of the vast majority of practical flow fields. There is no variation of the stagnation pressure between streamlines as deduced by consideration of the Lamb vector divergence, and furthermore, the Lamb vector curl, which quantifies the departure from circulation-preserving motions (including effects relating to the advection and stretching of vorticity), is also zero. To exclude such influential effects when developing models of vortical motions is not desirable, as these are the very mechanisms that drive momentum and energy transfer in turbulent flows.

5. Analysis

The instantaneous evolution of the Lamb vector divergence has direct connections to the transport of momentum and vorticity in turbulent flows. To complement the analytical examples discussed in the previous section, the dynamics of the Lamb vector divergence for turbulent channel and oscillating cylinder flow are now discussed.

5.1. *Turbulent channel flow*

The Lamb vector divergence may be separated into a mean $\Lambda = \overline{\nabla\cdot\boldsymbol{l}}$ and a fluctuating component with zero mean fluctuation $\lambda = (\nabla\cdot\boldsymbol{l})'$. Hence, for plane channel flow, the mean Lamb vector divergence is given by

$$\Lambda^+ = -U^+\frac{\mathrm{d}^2U^+}{\mathrm{d}y^{+2}} - \left(\frac{\mathrm{d}U^+}{\mathrm{d}y^+}\right)^2 + \frac{\mathrm{d}}{\mathrm{d}y^+}\left(\overline{u'\omega_z'}^+ - \overline{w'\omega_x'}^+\right). \tag{5.1}$$

In this expression, U is the mean streamwise velocity; u', v', and w' are the fluctuating velocity components in the streamwise direction x, wall-normal direction y, and spanwise direction z; and ω_k' is the fluctuating vorticity component in the k direction with mean spanwise vorticity $\Omega_z = -\mathrm{d}U/\mathrm{d}y$. A superscript + denotes that the quantity has been non-dimensionalized by the friction velocity u_τ and ν, e.g. $y^+ = yu_\tau/\nu$. To make the exposition more clear, the three terms in (5.1) are denoted by $F^+ = -U^+\mathrm{d}\Omega_z^+/\mathrm{d}y^+$, $E^+ = -\Omega_z^{+2}$, and $C^+ = \mathrm{d}(\overline{u'\omega_z'}^+ - \overline{w'\omega_x'}^+)/\mathrm{d}y^+$ as the mean flexion product, mean (negative) enstrophy, and mean velocity–vorticity correlation contributions, respectively. The mean Lamb vector divergence may then be expressed as the sum of three dynamically distinct mean quantities $\Lambda^+ = F^+ + E^+ + C^+$.

The inner normalized profiles of these quantities are shown in figure 2. The profiles shown in figure 2 are derived from the DNS of Moser, Kim & Mansour (1999). All derivatives were computed using the same Chebyshev collocation method of

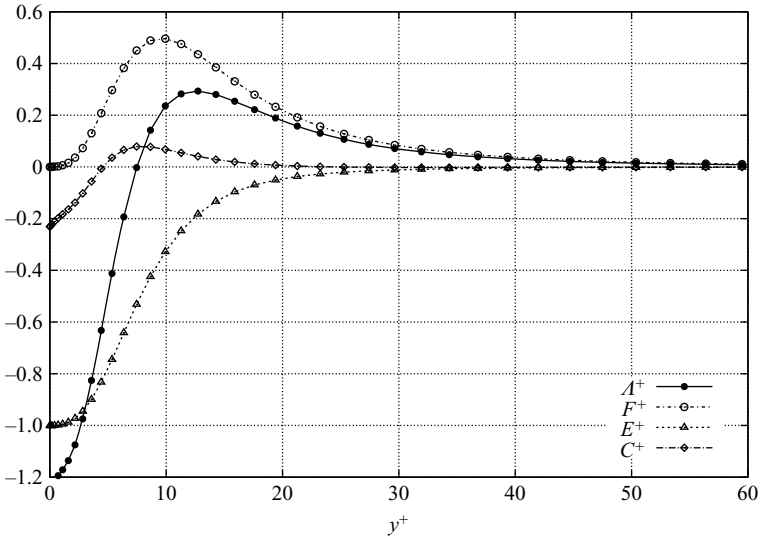

FIGURE 2. The mean Lamb vector divergence Λ^+, flexion product F^+, enstrophy E^+, and correlation C^+ profiles for the $Re_\tau = 590$ channel flow of Moser *et al.* (1999). For the range of data examined, these profiles exhibit little Reynolds number dependence.

Moser *et al.* (1999) to ensure spectral accuracy. The correlation term C^+ was determined through successive differentiation of the diagonal Reynolds stress components given in (5.3).

5.1.1. *Mean quantities*

As seen from figure 2, each term is symmetric with respect to the centreline and decays to zero outside the buffer layer. F^+ is strictly non-negative while E^+ is a monotonically increasing function throughout the channel half-width. C^+ has a similar profile to that of $F^+ + E^+$ alone although it is concentrated closer to the wall. C^+ also reaches a maximum at $y^+ \approx 7.5$ near the peak mean streamwise velocity curvature, $\mathrm{d}^2U^+/\mathrm{d}y^{+2}$, where Λ^+ is zero and the mean Bernoulli function transitions from a subharmonic to superharmonic state. The peak F^+ occurs at $y^+ \approx 10$ near the lower edge of the buffer layer, while the peak Lamb vector divergence occurs at $y^+ \approx 12$. These positions also coincide with an approximate balance between the viscous and Reynolds stress.

Manipulation of the y-component of the momentum equation for steady, fully developed, isochoric, plane turbulent channel flow reveals that (Klewicki 1989)

$$\overline{u'\omega_z'}^+ - \overline{w'\omega_x'}^+ = -\frac{1}{2}\frac{\mathrm{d}}{\mathrm{d}y^+}(\overline{u'u'}^+ - \overline{v'v'}^+ + \overline{w'w'}^+). \tag{5.2}$$

Therefore, the mean velocity–vorticity correlation is

$$C^+ = -\frac{1}{2}\frac{\mathrm{d}^2}{\mathrm{d}y^{+2}}(\overline{u'u'}^+ - \overline{v'v'}^+ + \overline{w'w'}^+). \tag{5.3}$$

The curvature of these diagonal Reynolds stress components, or normal stresses, contribute comparatively little to the magnitude of Λ^+, but the turbulent velocity fluctuations collectively act to enhance turbulent mixing and contract the subharmonic region closer to the wall relative to $F^+ + E^+$ alone.

Klewicki (1989) provides experimental data on the wall-normal variation of velocity–vorticity correlations for zero-pressure-gradient turbulent boundary layers. Figure 2 of that paper provides profiles of $\overline{u'\omega_z'}^+$. These show that for $7 < y^+ < 20$, $\overline{u'\omega_z'}^+ \propto \ln y^+$. As a result, the wall-normal gradient of $\overline{u'\omega_z'}^+$ is proportional to $1/y^+$ for $7 < y^+ < 20$. For $y^+ \geqslant 20$, this term decays to zero as corroborated by figure 2. The velocity–vorticity correlation $\overline{w'\omega_x'}^+$ exhibits less variation across the boundary layer than $\overline{u'\omega_z'}^+$. Thus, the wall-normal gradient of $\overline{w'\omega_x'}^+$ is conservatively bounded by the gradient of $\overline{u'\omega_z'}^+$.

The experimental data support the conclusion that the gradient of these velocity–vorticity correlations, C^+, is of little importance to the wall-normal distribution of the mean Lamb vector divergence throughout much of the inner layer – even for much higher Reynolds number flows than reflected by the data herein. This term does, however, play an important role in the transition layer where the leading order terms of Λ^+ sum to zero and C^+ is near a positive maximum. This acts to contract the Λ^+ distribution closer to the wall, thereby promoting turbulent mixing. Thus, the mean Lamb vector divergence is well approximated by

$$\Lambda^+ \approx -U^+ \frac{\mathrm{d}^2 U^+}{\mathrm{d}y^{+2}} - \left(\frac{\mathrm{d}U^+}{\mathrm{d}y^+}\right)^2, \tag{5.4}$$

for unidirectional turbulent shear flow as shown in figure 2.

The harmonic state of the mean Bernoulli function describes the relationship between locally large amplitude fluctuations about the mean and the intermittent effects they subsequently produce within the mean flow. The inflection point of the mean Bernoulli function, which is located where the mean Lamb vector divergence is zero, separates two distinct dynamical regions of the flow: the viscous sublayer and buffer layer. Hence, the flow in the subharmonic region (viscous sublayer) predominantly acts as a sink that stores the capacity to effect a momentum flux while the flow in the superharmonic region (buffer layer) acts to release momentum flux. Across this zone, there is an equal tendency for either momentum transport process to occur, and in particular, for a transfer of energy to occur between these regions. This process finds mathematical foundation in the advective terms of Lamb vector divergence transport equation. For example, $\boldsymbol{l} \cdot \nabla^2 \boldsymbol{u}$ represents this energy transfer process that occurs normal to the velocity field from the viscous sublayer to the buffer layer and vice versa. Such processes are discussed at greater length in § 5.1.4.

5.1.2. *Joint PDFs*

Further insights are gained by considering the joint probability density functions (PDFs) of the fluctuating Lamb vector divergence and associated quantities. We observe that the enstrophy fluctuations e^+ and flexion product fluctuations f^+ are generally uncorrelated. Additionally, in regions where e^+ is highly correlated with λ^+ (e.g. in the viscous sublayer), f^+ is typically uncorrelated with λ^+, while in regions where f^+ is highly correlated with λ^+ (e.g. in the buffer layer), e^+ is typically uncorrelated with λ^+.

Particularly interesting is that λ^+ is well correlated with the fluctuating Bernoulli function ϕ^+ in near-wall regions where Λ^+ is non-zero, as shown in figure 3. Furthermore, there exists a negative correlation in the viscous sublayer where the enstrophy dominates, while, in regions where the Lamb vector divergence is positive, λ^+ and ϕ^+ are positively correlated. Hence, in traversing from the sublayer to the buffer layer the nature of the correlation dramatically changes. At $y^+ = 2$, the

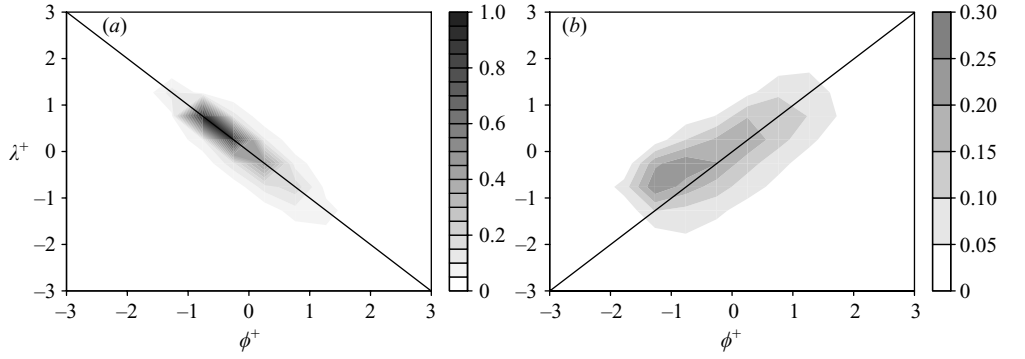

FIGURE 3. Normalized joint probability density function between λ^+ and ϕ^+ (*a*) in the viscous sublayer at $y^+ = 2$ and (*b*) in the buffer layer at $y^+ = 12$ for $Re_\tau = 180$ channel flow. The correlation coefficient is -0.93 at $y^+ = 2$ and 0.70 at $y^+ = 12$.

correlation coefficient between the Lamb vector divergence and Bernoulli function is a remarkable value of -0.93, with the dominant contributions coming from the second quadrant (positive λ^+, negative ϕ^+). Conversely, at $y^+ = 12$ the correlation between λ^+ and ϕ^+ is 0.70, with the bulk of the contributions coming from the third quadrant. This exceptionally strong variation in the correlation coefficient occurs over less than ten viscous lengths and, thus, sharply delineates the different physical mechanisms that drive the dynamics in the viscous sublayer and buffer layer.

Positive fluctuations of λ^+ in the viscous sublayer are accompanied by a net reduction of mechanical energy, while, in the buffer layer, positive fluctuations are accompanied by a net increase of mechanical energy. Furthermore, the joint PDFs demonstrate that, in the viscous sublayer, these positive fluctuations of λ^+ are due to enstrophy fluctuations, while in the buffer layer the positive fluctuations of λ^+ are due to fluctuating flexion product. In the viscous sublayer, these events are most strongly associated with negative energy fluctuations that arise due to strong negative enstrophy fluctuations. Similarly, the behaviour of the fluctuations in the buffer layer at the peak in Λ^+, where the flexion product is decreasing, corresponds to processes by which predominantly high-momentum fluid parcels have expended their energy in accelerating the surrounding fluid, thereby promoting negative flexion product fluctuations, and hence reduced momentum flux. Regions of positive flexion product do contribute to local viscous losses in mechanical energy in the buffer layer; however, the viscous time scales are longer than the associated inertial scales such that these regions overwhelmingly redistribute momentum to the surroundings. This analysis provides a basis, supported by simulation data with an analytical foundation, to connect the mean Lamb vector divergence distribution to the local fluctuations that drive turbulent mixing. The reciprocating interaction between positive and negative regions of Lamb vector divergence is, in all likelihood, generic to the processes by which dynamically relevant motions effect a time rate of change of momentum.

5.1.3. *Relationship to the mean momentum balance*

For pressure-driven channel flow, the differential mean force balance is

$$0 = \frac{1}{\delta^+} + \frac{\mathrm{d}^2 U^+}{\mathrm{d}y+^2} - \frac{\mathrm{d}\overline{u'v'}^+}{\mathrm{d}y^+}, \tag{5.5}$$

where $1/\delta^+$ is the normalized mean pressure gradient, $\mathrm{d}^2U^+/\mathrm{d}y^{+2}$ is the mean viscous stress gradient, and the last term is the gradient of the Reynolds stress. As given by Klewicki (1989), the Reynolds stress gradient for fully developed incompressible turbulent channel flow may be written in terms of velocity–vorticity correlations as

$$\frac{\mathrm{d}\overline{u'v'}^+}{\mathrm{d}y^+} = \overline{w'\omega_y'}^+ - \overline{v'\omega_z'}^+ = \overline{l_x}^+, \tag{5.6}$$

where the streamwise Lamb vector is identically $l_x = w\omega_y - v\omega_z$.

Wei *et al.* (2005) have shown that, to lowest order, the balance expressed by (5.5) is described by a four-layer structure. The streamwise Lamb vector component is a leading term in (5.5) that establishes the balance in layers II, III and IV, i.e. outside the viscous sublayer. On the other hand, the mean spanwise Lamb vector is identically zero so that $\overline{l_z} = \overline{v'\omega_x'} - \overline{u'\omega_y'} = 0$ for fully developed turbulent channel flow. The mean wall-normal component of the Lamb vector is given by

$$\overline{l_y} = U\Omega_z + \overline{u'\omega_z'} - \overline{w'\omega_x'}. \tag{5.7}$$

Thus, $\overline{l_y}$ is the only Lamb vector component that contains the mean velocity and vorticity in addition to velocity–vorticity correlations. Furthermore, the mean wall-normal Lamb vector is equal to the wall-normal gradient of the mean Bernoulli function, and hence the wall-normal gradient of $\overline{l_y}$ is the mean Lamb vector divergence. This suggests that the Lamb vector and, in particular, the Lamb vector divergence are particularly relevant to the mean momentum balance.

As described by Klewicki *et al.* (2007), layer II is where the Reynolds and viscous stress gradients balance. This layer is primarily composed of separated pockets of low- and high-energy fluid. The interaction between these regions of flow drives the self-sustaining mechanisms of near-wall turbulence; however, this process would not repeat if not for the introduction of sufficient high-momentum fluid from the bulk flow to interact with the low-speed, high-vorticity fluid near the wall. Negative Reynolds stress gradients in layer IV introduce high-momentum fluid to layer II. This inner–outer interaction injects an imbalance in the underlying energy distribution and, as a result, pockets of concentrated and depleted flow energy are formed in layer II. The mechanisms associated with the Lamb vector divergence play an important role in establishing this mean momentum balance layer structure, particularly through the inner–outer interactions across layer III that feed layer II. These connections, however, require further investigation.

To a first-order approximation, the mean Lamb vector divergence transport equation for fully developed turbulent channel flow is identically the mean streamwise force balance multiplied by the viscous force term, or mean flow curvature, i.e. $\mathrm{d}^2U/\mathrm{d}y^2$. Hence, the Lamb vector divergence transport equation is the streamwise force balance attenuated or amplified by the curvature of the velocity field. The Lamb vector divergence then identifies the forces that have a disproportionate ability to alter the mean momentum balance, or equivalently, redistribute momentum in regions where there is high-flow curvature (e.g. in subharmonic or superharmonic regions). Consequentially, if one thinks of the amplified mean curvature of the turbulent boundary layer (relative to the laminar boundary layer) as being driven by the macroscopic stirring of momentum then, in effect, the Lamb vector and the Lamb vector divergence are the fundamental mechanisms that drive energy, momentum and vorticity transfer between the inner and outer layers.

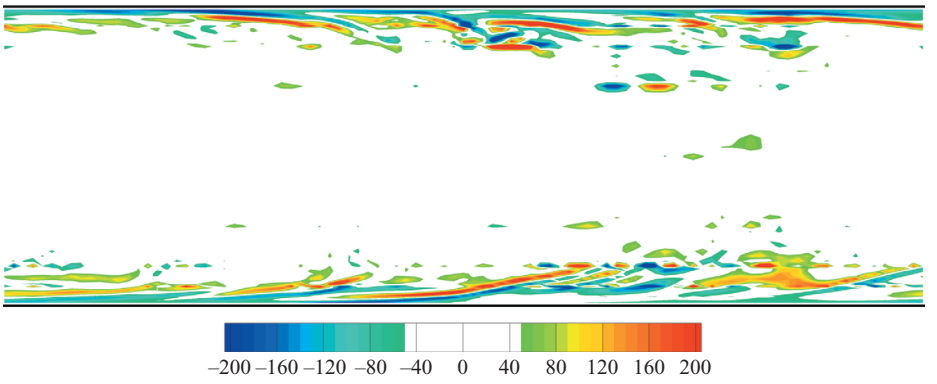

FIGURE 4. Instantaneous x–y cross-section of the Lamb vector divergence for turbulent channel flow at $Re_\tau = 180$ non-dimensionalized by the channel half-height and mean centreline velocity. The flow is from left to right. Scale does not include the entire range.

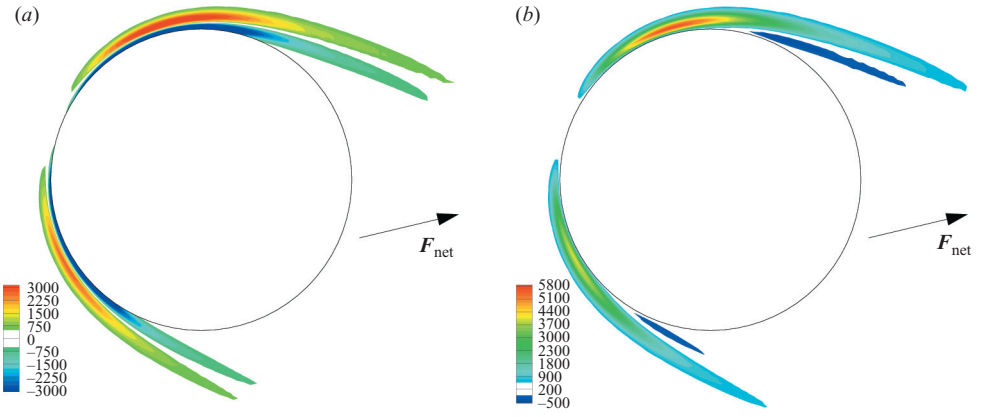

FIGURE 5. Instantaneous cross-section of the (a) Lamb vector divergence and (b) flexion product distributions of a circular cylinder in vortex-induced vibration at $Re_D = 720$ and $V_r = 6.5$ non-dimensionalized by the cylinder diameter and free-stream velocity. The flow is from left to right. The total resultant force is directed as shown. Scale does not include the entire range.

5.1.4. *Instantaneous turbulent channel flow dynamics*

A representative, instantaneous x–y cross-section of the Lamb vector divergence for plane channel flow is shown in figure 4. These results provide an opportunity to construct interpretations consistent with previous empirical observations. For example, the transient behaviour within the viscous sublayer is predominantly composed of regions of low-momentum fluid separated by small sheets of high-momentum fluid indicative of sweep-like motions consistent with a subharmonic Bernoulli function and negative Lamb vector divergence. Conversely, the behaviour in the buffer layer immediately above the transition from negative to positive mean Lamb vector divergence consists primarily of high-momentum fluid surrounded by sheets of low-momentum fluid characteristic of ejections and a superharmonic Bernoulli function. Like ejections and sweeps, negative regions of Lamb vector divergence typically precede positive regions (Offen & Kline 1975). The temporal interactions between

these dynamically distinct regions of Lamb vector divergence embody how ejections and sweeps perturb the wall layer away from a harmonic state thereby enhancing turbulent mixing, as described in § 3.

Regions of negative Lamb vector divergence act to enhance the potential energy of a vortical motion due to the topological configuration of the momentum flux. These regions of local momentum flux minima are subsequently converted to momentum flux maxima through interaction with the surrounding high-momentum fluid and corresponding depletion of the low-pressure zone associated, for example, with a vortex-like motion. This process repeats itself as the momentum flux is depleted in the positive regions, thereby returning the flow to a harmonic state. Hence, there exists a quasi-cyclic behaviour between regions of negative and positive Lamb vector divergence, which is intimately related to the momentum transport mechanisms in turbulent flows and readily understood by consideration of the dynamical terms of (3.6). Several studies (e.g. Robinson 1991, and numerous references therein) have observed this quasi-cyclic behaviour of coherent motions that is naturally described by the Lamb vector divergence.

5.2. *Oscillating cylinder flow*

As a second instantaneous flow example, we now consider the flow around the oscillating cylinder shown in figure 5. This particular three-dimensional cylinder flow is similar to that given by Blackburn, Govardhan & Williamson (2001), where a circular cylinder oscillates due to vortex-induced vibration with uniform upstream flow. In this example, the Lamb vector divergence, flexion product, and enstrophy have significant dynamical range within the cylinder boundary layer. The stagnation point at the leading edge of the cylinder is a region of zero Lamb vector divergence, as figure 5(*a*) demonstrates. This is a consequence of the zero-vorticity stagnation-point flow in that region. In contrast, the flexion product shown in figure 5(*b*) marks the beginning of separation, as the location where the flexion product changes sign from positive under a decreasingly favourable pressure gradient to negative under an increasingly adverse pressure gradient. In this flow, the flexion product is predominantly positive. Negative flexion product, however, can appear in regions of separated flow and within the wake where u^2 is subharmonic.

Recalling the discussion of § 2.2, the net force has both drag and lift components as indicated in figure 5. This force is not parallel to the free-stream velocity since the oscillatory motion is near the maximum positive velocity phase so that the pressure on the upper half of the cylinder is less than that on the lower half, leading to lift. Since the Lamb vector divergence is concentrated more intensely over a wider region along the upper half of the cylinder, (2.6) also predicts this upward lift force. Furthermore, the Lamb vector divergence becomes increasingly localized around the cylinder wall as the Reynolds number increases; as a result, the observed drag reduction beyond the critical Reynolds number is reflected by the spatial variations of the Lamb vector divergence.

6. Discussion

By directly connecting the Lamb vector divergence to the underlying dynamical equations, a foundation for identifying and studying dynamically significant motions was developed. Several physical and theoretical properties of the Lamb vector divergence were presented; implications of this analysis are now briefly discussed.

6.1. *Physical implications*

The Lamb vector divergence has been shown to identify those motions that have the capacity to effect a time rate of change of momentum. The Lamb vector divergence transport equation captures the mechanisms by which spatial variations in this capacity interact and evolve. Each term in the transport equation accommodates a distinct physical interpretation, collectively sustaining a quasi-cyclic exchange of momentum between regions of high- and low-momentum fluid. The viscous terms act to harmonize the Bernoulli function, thereby minimizing the momentum flux curvature. Conversely, the advective terms counteract this minimization process and force the flow to either a subharmonic or superharmonic state. Through the action of the flexion product advective terms, an initially subharmonic, or low-momentum, fluid parcel's angular momentum is converted into concentrated momentum flux, thereby transitioning the flow to a superharmonic state. Similarly, the advective enstrophy terms counteract this progression by acting to return the flow to a subharmonic state. The regenerative nature and dynamical significance of these physical mechanisms are strongly connected to the attributes commonly associated with coherent motions.

Indeed, for the case of turbulent channel flow, analysis of the Lamb vector divergence transport equation leads to a refined interpretation of wall-layer sweep and ejection phenomena. As demonstrated in § 5.1, the viscous sublayer is predominantly composed of regions of low-momentum fluid separated by small sheets of high-momentum fluid indicative of subharmonic sweeps. In contrast, the buffer layer is characterized by high-momentum fluid surrounded by sheets of low-momentum fluid indicative of superharmonic ejections. The transition between regions of negative and positive Lamb vector divergence corresponds to a distinct change in the overall flow dynamics, e.g. when traversing from the viscous sublayer to the buffer layer. Therefore, the Lamb vector divergence captures the temporal evolution of regions of high- and low-momentum fluid, which is directly related to the mechanisms that drive turbulent mixing.

From the dynamical properties of the Lamb vector divergence, a framework for addressing drag reduction in bluff body flows was obtained. A number of potential methods to control drag production by separating geometric and dynamical factors were identified in § 2.2. For example, harmonizing the Bernoulli function or balancing the spatial distribution of positive and negative Lamb vector divergence leads to drag reduction. Since the Lamb vector divergence only requires measurement of the velocity field and its derivatives, analysis of such is experimentally feasible. Therefore, this dynamical quantity is open to study and investigation as a diagnostic tool in physical experiments. Of particular interest relative to drag studies is that the locality of the Lamb vector divergence often allows one to ignore the far field and focus only on the regions immediately surrounding the bluff body to determine the pressure drag. Thus, the resultant drag force on bluff bodies can be computed from the Lamb vector divergence distribution with reasonable experimental and computational effort. Furthermore, the tendency for the Lamb vector divergence to concentrate suggests that modelling the Lamb vector divergence distribution can lead to improved drag reduction methodologies.

6.2. *Theoretical implications*

The Lamb vector divergence provides a rigorous foundation for the analysis of momentum and energy transfer in turbulent flows. The preceding analysis has revealed the mechanisms by which high- and low-momentum fluid packets interact: regions of negative Lamb vector divergence represent spatially localized motions that have

accumulated a capacity to effect a time rate of change of momentum while positive regions represent motions that have a depleted capacity in this regard. Since the Lamb vector divergence provides a physically relevant and well-defined classification of the incipient dynamics, visualization methods that extract zones of positive and negative Lamb vector divergence and follow their temporal evolution, as described by the Lamb vector divergence transport equation, are well suited to further analysis and warrant future investigation.

Positive flexion product identifies the redistribution of high-energy content fluid so as to accelerate the surrounding low-speed fluid. Qualitatively, this may be associated with the unwinding of a vortex, i.e. the conversion of the angular momentum stored in a rotational, or subharmonic, motion into linear momentum accompanied by a corresponding depletion of the low-pressure zone. The interference between the flexion product and enstrophy dictates the character of the Bernoulli function, and hence controls the harmonization of the Bernoulli function. Exploration of these mechanisms holds significant potential for analysis in several other research areas. These include magnetohydrodynamic flows, where the interference between the Lamb vector and Lorentz force divergence yields an analogous source–sink decomposition, and acoustics, where the Lamb vector divergence appears as a dominant source term in Lighthill's wave equation.

Equation (2.7) demonstrates that the total kinetic energy is directly related to a weighted volume integral of the Lamb vector divergence. Furthermore, for a non-trivial class of motions, the average Lamb vector divergence given by a non-weighted volume integral is zero. This then implies a global balance between the flexion product and enstrophy, and hence the flow dynamics naturally promote harmonization of the Bernoulli function, or equivalently, act to minimize the energy curvature. It is, however, the local variations between regions of positive and negative Lamb vector divergence that propagate energy and redistribute momentum throughout the flow. This process is rigorously described via the self-interaction of the competing flexion product and enstrophy advective terms found in the Lamb vector divergence transport equation.

This work was partially supported by the NSF grant CBET-0555223 (grant monitor W. Schultz). The third author acknowledges the support of NSF Career Award CCF-0347791. The authors gratefully acknowledge Drs Bhattacharjee, Brasseur, Marmanis and Sherwin for many fruitful discussions. We would also like to thank Dr Blackburn for providing his DNS channel and cylinder flow data as well as Drs Moser, Kim and Mansour for making their DNS data publicly available.

REFERENCES

Adrian, R. J. & Moin, P. 1988 Stochastic estimation of organized turbulent structure: Homogeneous shear flow. *J. Fluid Mech.* **190**, 531–559.

Alim, A. 2007 A physical comprehensive definition of a vortex based on the Lamb vector. *Algerian J. Appl. Fluid Mech.* **1**, 1–5.

Aubry, N., Holmes, P., Lumley, J. L. & Stone, E. 1988 The dynamics of coherent structures in the wall region of a turbulent boundary layer. *J. Fluid Mech.* **192**, 115–173.

Bakewell, H. P. & Lumley, J. L. 1967 Viscous sublayer and adjacent wall region in turbulent pipe flow. *Phys. Fluids* **10**, 1880–1889.

Batchelor, G. K. 1953 *The Theory of Homogeneous Turbulence*. Cambridge University Press.

Batchelor, G. K. 1967 *An Introduction to Fluid Dynamics*. Cambridge University Press.

Berkooz, G., Holmes, P. & Lumley, J. L. 1991 Intermittent dynamics in simple models of the turbulent wall layer. *J. Fluid Mech.* **230**, 75–95.

Berkooz, G., Holmes, P. & Lumley, J. L. 1993 The proper orthogonal decomposition in the analysis of turbulent flows. *Annu. Rev. Fluid Mech.* **25**, 539–575.

Blackburn, H. M., Govardhan, R. & Williamson, C. H. K. 2001 A complementary numerical and physical investigation of vortex-induced vibration. *J. Fluids Struct.* **15**, 481–488.

Brasseur, J. G. & Lin, W. 2005 Kinematics and dynamics of small-scale vorticity and strain-rate structures in the transition from isotropic to shear turbulence. *Fluid Dyn. Res.* **36**, 357–384.

Chakraborty, P., Balachandar, S. & Adrian, R. J. 2005 On the relationships between local vortex identification schemes. *J. Fluid Mech.* **535**, 189–214.

Chambers, D. H., Adrian, R. J., Stewart, D. S. & Sung, H. J. 1988 Karhunen–Loéve expansion of Burgers' model of turbulence. *Phys. Fluids* **31**, 2573–2582.

Choi, H., Moin, P. & Kim, J. 1993 Direct numerical simulation of turbulent flow over riblets. *J. Fluid Mech.* **255**, 503–539.

Crawford, C. H., Marmanis, H. & Karniadakis, G. E. 1998 The Lamb vector and its divergence in turbulent drag reduction. In *Proc. Intl Symposium on Seawater Drag Reduction*, pp. 99–107.

Dombre, T., Frisch, U., Greene, J. M., Henon, M., Mehr, A. & Soward, A. M. 1986 Chaotic streamlines in the ABC flows. *J. Fluid Mech.* **167**, 353–391.

Ferrante, A. & Elghobashi, S. 2004 On the physical mechanisms of drag reduction in a spatially developing turbulent boundary layer laden with microbubbles. *J. Fluid Mech.* **503**, 345–355.

Hinze, J. O. 1975 *Turbulence*. McGraw-Hill.

Howe, M. S. 1975 Contributions to the theory of aerodynamic sound, with application to excess jet noise and the theory of the flute. *J. Fluid Mech.* **71**, 625–673.

Jeong, J. & Hussain, F. 1995 On the identification of a vortex. *J. Fluid Mech.* **285**, 69–94.

Klewicki, J. C. 1989 Velocity–vorticity correlations related to the gradients of the Reynolds stresses in parallel turbulent wall flows. *Phys. Fluids* A **1**, 1285–1288.

Klewicki, J. C., Fife, P., Wei, T. & McMurtry, P. A. 2007 A physical model of the turbulent boundary layer consonant with mean momentum balance structure. *Phil. Trans. R. Soc. Lond.* **365**, 823–839.

Klewicki, J. C. 1998 Connecting vortex regeneration with near-wall stress transport. In *AIAA Paper* 1998-2963.

Kollmann, W. 2006 Critical points and manifolds of the Lamb vector field in swirling jets. *Comput. Fluids* **35**, 746–754.

Küchemann, D. 1965 Report on the IUTAM symposium on concentrated vortex motions in fluids. *J. Fluid Mech.* **21**, 1–20.

Lighthill, M. J. 1952 On sound generated aerodynamically. Part I. *Proc. R. Soc. Lond.* A **211**, 564–587.

Lumley, J. L. 1967 The structure of inhomogeneous turbulent flows. In *Atmospheric Turbulence and Radio Wave Propagation* (ed. A. M. Yaglom & V. I. Tatarsky), pp. 166–178. Nauka, Moscow.

Marcu, B., Meiburg, E. & Newton, P. K. 1994 Dynamics of heavy particles in a Burgers vortex. *Phys. Fluids* **7**, 400–410.

Marmanis, H. 1998 Analogy between the Navier–Stokes equations and Maxwell's equations: Application to turbulence. *Phys. Fluids* **10**, 1428–1437.

Moffatt, H. K. & Tsinober, A. 1992 Helicity in laminar and turbulent flow. *Annu. Rev. Fluid Mech.* **24**, 281–312.

Moffatt, H. K. 1985 Magnetostatic equilibria and analogous Euler flows of arbitrarily complex topology. Part 1. Fundamentals. *J. Fluid Mech.* **159**, 359–378.

Moffatt, H. K. 1986*a* Magnetostatic equilibria and analogous Euler flows of arbitrarily complex topology. Part 2. Stability considerations. *J. Fluid Mech.* **166**, 359–378.

Moffatt, H. K. 1986*b* On the existence of localized rotational disturbances which propagate without change of structure in an inviscid fluid. *J. Fluid Mech.* **173**, 289–302.

Monin, A. & Yaglom, A. 1977 *Statistical Fluid Mechanics*. MIT Press.

Moser, R. D., Kim, J. & Mansour, N. N. 1999 Direct numerical simulation of turbulent channel flow up to $Re_\tau = 590$. *Phys. Fluids* **11**, 943–945.

Offen, G. R. & Kline, S. J. 1975 A proposed model of the bursting process in turbulent boundary layers. *J. Fluid Mech.* **70**, 209–228.

Protas, B. & Wesfreid, J. E. 2001 Drag force in the open-loop control of the cylinder wake in the laminar regime. *Phys. Fluids* **14**, 810–826.

Robinson, S. K. 1991 Coherent motions in turbulent boundary layers. *Annu. Rev. Fluid Mech.* **23**, 601–639.

Rousseaux, G., Seifer, S., Steinberg, V. & Wiebel, A. 2007 On the Lamb vector and the hydrodynamic charge. *Exps. Fluids* **42**, 291–299.

Shiels, D. & Leonard, A. 2001 Investigation of a drag reduction on a circular cylinder in rotary oscillation. *J. Fluid Mech.* **431**, 297–322.

Sposito, G. 1997 On steady flows with Lamb surfaces. *Intl J. Engng Sci.* **35**, 197–209.

Taylor, G. I. 1935 Statistical theory of turbulence. *Proc. R. Soc. Lond.* **151**, 421–444.

Truesdell, C. 1951 A form of Green's transformation. *Am. J. Maths* **73**, 43–47.

Truesdell, C. 1954 *The Kinematics of Vorticity*. Indiana University Press.

Tsinober, A. 1990 On one property of Lamb vector in isotropic turbulent flow. *Phys. Fluids* **2**, 484–486.

Tsinober, A. 1998 Is concentrated vorticity that important? *Eur. J. Mech.* B **17**, 421–449.

Tsinober, A. & Levich, E. 1983 On the helical nature of three dimensional coherent structures in turbulent flows. *Phys. Rev. Lett.* A **99**, 321–323.

Wei, T., Fife, P., Klewicki, J. & McMurtry, P. 2005 Properties of the mean momentum balance in turbulent boundary layer, pipe and channel flows. *J. Fluid Mech.* **522**, 303–327.

Wu, J.-Z., Ma, H.-Y. & Zhou, M.-D. 2006 *Vorticity and Vortex Dynamics*. Springer.

Xu, J., Maxey, M. R. & Karniadakis, G. E. 2002 Numerical simulation of turbulent drag reduction using micro-bubbles. *J. Fluid Mech.* **468**, 271–281.

Yang, Y. T., Zhang, R. K., An, Y. R. & Wu, J. Z. 2007 Steady vortex force theory and slender-wing flow diagnosis. *Acta Mechanica Sinica* **23**, 609–619.